ARTICLE

RINT1 Bi-allelic Variations Cause Infantile-Onset Recurrent Acute Liver Failure and Skeletal Abnormalities

Margot A. Cousin,[1,2,18] Erin Conboy,[1,3,18] Jian-She Wang,[4,5,18] Dominic Lenz,[6,18] Tanya L. Schwab,[1,7] Monique Williams,[7] Roshini S. Abraham,[8] Sarah Barnett,[9] Mounif El-Youssef,[10] Rondell P. Graham,[9] Luz Helena Gutierrez Sanchez,[10] Linda Hasadsri,[9] Georg F. Hoffmann,[6] Nathan C. Hull,[11] Robert Kopajtich,[12,13] Reka Kovacs-Nagy,[12,13] Jia-qi Li,[4] Daniela Marx-Berger,[14] Valérie McLin,[15] Mark A. McNiven,[7,16] Taofic Mounajjed,[9] Holger Prokisch,[12,13] Daisy Rymen,[17] Ryan J. Schulze,[7,16] Christian Staufner,[6] Ye Yang,[4] Karl J. Clark,[1,7] Brendan C. Lanpher,[1,3,*] and Eric W. Klee[1,2,3,9,*]

Pediatric acute liver failure (ALF) is life threatening with genetic, immunologic, and environmental etiologies. Approximately half of all cases remain unexplained. Recurrent ALF (RALF) in infants describes repeated episodes of severe liver injury with recovery of hepatic function between crises. We describe bi-allelic RINT1 alterations as the cause of a multisystem disorder including RALF and skeletal abnormalities. Three unrelated individuals with RALF onset ≤3 years of age have splice alterations at the same position (c.1333+1G>A or G>T) in trans with a missense (p.Ala368Thr or p.Leu370Pro) or in-frame deletion (p.Val618_Lys619del) in RINT1. ALF episodes are concomitant with fever/infection and not all individuals have complete normalization of liver function testing between episodes. Liver biopsies revealed nonspecific liver damage including fibrosis, steatosis, or mild increases in Kupffer cells. Skeletal imaging revealed abnormalities affecting the vertebrae and pelvis. Dermal fibroblasts showed splice-variant mediated skipping of exon 9 leading to an out-of-frame product and nonsense-mediated transcript decay. Fibroblasts also revealed decreased RINT1 protein, abnormal Golgi morphology, and impaired autophagic flux compared to control. RINT1 interacts with NBAS, recently implicated in RALF, and UVRAG, to facilitate Golgi-to-ER retrograde vesicle transport. During nutrient depletion or infection, Golgi-to-ER transport is suppressed and autophagy is promoted through UVRAG regulation by mTOR. Aberrant autophagy has been associated with the development of similar skeletal abnormalities and also with liver disease, suggesting that disruption of these RINT1 functions may explain the liver and skeletal findings. Clarifying the pathomechanism underlying this gene-disease relationship may inform therapeutic opportunities.

Introduction

Acute liver failure (ALF) in infancy and childhood is a severe, life-threatening condition with a wide differential diagnosis that includes infection, toxin exposure, autoimmune disease, shock, inherited metabolic disease, and several other rare etiologies. This condition is defined by acute onset of liver disease with hepatic-based coagulopathy (PT > 20 s, or INR > 2) not corrected by parenteral vitamin K with or without hepatic encephalopathy (HE) or coagulopathy (PT 15–19.9, INR 1.5–1.9) with HE.[1] Nearly half of pediatric cases remain unexplained despite diagnostic evaluation. Reports of recurrent acute liver failure (RALF) in infants describe repeated episodes of severe injury with recovery of hepatic function. Heritable etiologies of RALF include mitochondrial disorders, Wolcott-Rallison syndrome (MIM: 226980), autoimmune hepatitis, and bi-allelic pathogenic variations in dihydrolipoamide dehydrogenase (DLD [MIM: 246900]) and leucyl-tRNA synthetase (LARS [MIM: 615438]) genes, among others.[1,2]

Haack et al. reported a series of individuals with bi-allelic variants in neuroblastoma-amplified sequence (NBAS [MIM: 608025]) leading to RALF. This liver failure disorder, with onset in infancy and ALF precipitated by febrile illness, is now termed infantile liver failure syndrome, type 2 (MIM: 616483).[3] Whole-exome sequencing (WES) revealed bi-allelic NBAS variants in ten unrelated individuals with fever-dependent RALF. The initial report was followed by further description of the phenotypic spectrum, disease mechanism, and therapeutic concepts[4] as well as

[1]Center for Individualized Medicine, Mayo Clinic, Rochester, MN 55905, USA; [2]Department of Health Sciences Research, Mayo Clinic, Rochester, MN 55905, USA; [3]Department of Clinical Genomics, Mayo Clinic, Rochester, MN 55905, USA; [4]Department of Pediatrics, Jinshan Hospital, Fudan University, 201508 Shanghai, China; [5]Center for Pediatric Liver Diseases, Children's Hospital of Fudan University, 201102 Shanghai, China; [6]Department of General Pediatrics, Division of Neuropediatrics and Pediatric Metabolic Medicine, University Hospital Heidelberg, Im Neuenheimer Feld 430, 69120 Heidelberg, Germany; [7]Department of Biochemistry and Molecular Biology, Mayo Clinic, Rochester, MN 55905, USA; [8]Department of Pathology and Laboratory Medicine, Nationwide Children's Hospital, Columbus, OH 43205, USA; [9]Department of Laboratory Medicine and Pathology, Mayo Clinic, Rochester, MN 55905, USA; [10]Department of Pediatric Gastroenterology and Hepatology, Mayo Clinic, Rochester, MN 55905, USA; [11]Department of Radiology, Division of Pediatric Radiology, Mayo Clinic, Rochester, MN 55905, USA; [12]Institute of Human Genetics, Helmholtz Zentrum München, 85764 Neuherberg, Germany; [13]Institute of Human Genetics, Technische Universität München, 81675 Munich, Germany; [14]Pediatric Nephrology, University Children's Hospital Zurich, Steinwiesstrasse 75, 8032 Zurich, Switzerland; [15]Pediatric Gastroenterology Unit, University Hospitals Geneva, Rue Willy-Donzé 6, 1211 Geneva, Switzerland; [16]Division of Gastroenterology and Hepatology, Mayo Clinic, Rochester, MN 55905, USA; [17]Department of Metabolic Diseases, University Children's Hospital Zurich, Zurich, Switzerland
[18]These authors contributed equally to this work
*Correspondence: lanpher.brendan@mayo.edu (B.C.L.), klee.eric@mayo.edu (E.W.K.)
https://doi.org/10.1016/j.ajhg.2019.05.011.

by additional reports of affected individuals.[5–7] NBAS interacts with ZW10 (MIM: 603954) and RAD50-interacting protein 1 (RINT1 [MIM: 610089]) in the NRZ complex. In association with p31 (USE1 [MIM: 610675]), the NRZ complex assembles with the N-ethylmaleimide-sensitive factor attachment protein receptor (SNARE) complex that is necessary for appropriate docking and fusion of transport vesicles in the endoplasmic reticulum and Golgi apparatus.[4,8] RINT1 has not been clearly associated with any human disease and bi-allelic pathogenic variants in RINT1 have not been described.

We describe three children with RALF and skeletal abnormalities who were found by WES to have compound heterozygous alterations in RINT1. We propose that RINT1 bi-allelic pathogenic variations cause a previously unrecognized disorder with features of RALF similar to NBAS deficiency but also with distinctive skeletal findings resembling a lysosomal storage disorder.

Subjects and Methods

Research Consent

All procedures followed were in accordance with the ethical standards of the responsible committee on human experimentation (institutional and national) and with the Helsinki Declaration of 1975, as revised in 2000. The families included in this study provided written informed consent to this research and publication under a protocol approved by the Mayo Clinic Institutional Review Board for family 1, under a protocol approved by the Institutional Review Board of Jinshan Hospital of Fudan University for family 2, and under an approved study by the ethics committees of the University Hospital Heidelberg and the Technische Universität München for family 3.

Genetic Analysis

Family 1

Clinical WES was performed on the proband, biological mother, and biological father by the Department of Laboratory Medicine and Pathology at Mayo Clinic in Rochester, Minnesota, USA. Genomic DNA was extracted from blood from the trio; 97% of the target exome was covered at a read depth of 20× or greater. The exome was captured utilizing a custom reagent developed by Mayo Clinic and Agilent Technologies, targeting 19,456 genes and 187,715 exons using 637,923 probes to capture a 54.1 Mbp total region. Sequencing was performed on an Illumina HiSeq 2500 Next Generation sequencing instrument, using HapMap Sample NA12878 as an internal control. Paired-end 101 base-pair reads were aligned to a modified human reference genome (GRCh37/hg19) using Novoalign (Novocraft Technologies, Malaysia). Sequencing quality was evaluated using FastQC. All germline variants were jointly called through GATK Haplotype Caller and GenotypeGVCF.[9] Each variant was annotated using the BioR Toolkit[10] and subsequently evaluated for clinical relevance. Targeted Sanger sequencing was used to confirm the reported variants identified by WES testing.

Family 2

WES, annotation, and filtering procedures were performed in proband 2 as described previously.[11] Sequencing and primary annotation were done by Genesky Shanghai Science & Tech Co,

Ltd. 6.0 Gb of sequences mapped to the reference genome corresponding to a 37.9-fold average coverage, with more than 76.9% of the target region covered at least 10-fold. After the compound heterozygous variants in RINT1 were identified in the affected child in family 1, a review of the sequence data of the proband in family 2 found two predicted pathogenic variants in RINT1. The two variants were verified through PCR (2*Master Mix, Cat. KT201, Tiangen China) followed by Sanger sequencing in the child and her parents (Figure S1).

Family 3

DNA of the affected child and her parents were examined in Munich by WES as described previously[12] using the Agilent SureSelect Human All Exon V6 kit followed by sequencing as 100-bp paired-end reads on an Illumina HiSeq4000. After alignment to the human reference genome (UCSC Genome Browser build hg19) using Burrows-Wheeler Aligner (BWA, v.0.7.5a),[13] single-nucleotide variants (SNVs) and small insertions and deletions (indels) were detected using SAMtools (v.0.1.19)[14] and GATK (v.3.8).[9] 11.5–12.6 Gb of sequences mapped to the reference genome corresponding to a 118- to 131-fold coverage, with more than 98.5% of the target region being covered at least 20-fold. Assuming a recessive type of inheritance, we filtered for rare likely pathogenic variants (MAF < 0.1% in an in-house and public databases), which prioritized compound heterozygous variants in RINT1.

Liver Pathology

Archived diagnostic slides from liver biopsies from each affected individual were reviewed by a clinical pathologist at Mayo Clinic.

Skeletal Images

Complete skeletal surveys from probands 1 and 2, and a subset of skeletal radiographical images from proband 3, were reviewed by a clinical radiologist at Mayo Clinic.

Fibroblast Cell Culture

Primary dermal fibroblast cultures were generated from skin biopsies from probands 1 and 3 and also from an individual with an unrelated genetic disorder as a control for the RNA sequencing experiment. The biopsies were minced and transferred to a T-25 culture flask for culture. Normal control fibroblasts (GM08429, Coriell Institute) were obtained for protein studies. The fibroblast cultures were maintained in minimal essential media supplemented with 10% fetal bovine serum, 1% non-essential amino acids, and 1% antibiotic/antimycotic and incubated at 37°C with 5% CO_2 and 5% O_2.

Whole-Transcriptome Sequencing of Fibroblasts

At ~50% confluency, fibroblasts from proband 1 and the control subject (individual with an unrelated genetic disorder) were trypsinized and replated into a T-75 flask. Once the T-75 reached 80%–90% confluency, the cells were harvested for RNA. For translation inhibition, 6 h before harvesting, the cultured fibroblasts were incubated with puromycin readymade solution (Sigma Aldrich), at a final concentration of 100 μg/mL. Cells from flasks untreated and treated with puromycin were scraped, counted, resuspended in 0.75 mL of Qiazol solution (QIAGEN) for 0.25 mL of sample, and frozen at −80°C. RNA was isolated using the miRNeasy Mini Kit (QIAGEN) following the standard protocol.

RIN and DV200 values were determined for starting RNA using the Agilent Bioanalyzer or Tapestation. RNA libraries were

prepared according to the manufacturer's instructions for the TruSeq RNA Access Library Prep Kit (Illumina). Coding regions of the transcriptome were captured by pooling four of the cDNA libraries at 200 ng each following the manufacturer's instructions for the TruSeq RNA Access Library Prep Kit (Illumina). The concentration and size distribution of the final libraries were determined on an Agilent Bioanalyzer DNA 1000 chip. A final quantification, using Qubit fluorometry (Invitrogen), was performed to confirm sample concentration.

Libraries were sequenced at ~75 million fragment reads per sample (4 samples/lane) following Illumina's standard protocol using the Illumina cBot and HiSeq 3000/4000 PE Cluster Kit. The flow cells were sequenced as 100 × 2 paired-end reads on an Illumina HiSeq 4000 using HiSeq 3000/4000 sequencing kit and HCS v3.3.20 collection software. Base-calling was performed using Illumina's RTA v.2.5.2.

RNA-sequencing analysis was performed using MAP-RSeq.[15] Reads were aligned to the human genome (hg19) and transcriptome using Tophat2[16] running Bowtie (v1).[17] Gene and exon level read counts were generated using HiSeq[18] and BedTools,[19] respectively.

RINT1, NBAS, and p31 Western Blot and 18 h 40°C Temperature Challenge

Fibroblasts from probands 1 and 3 as well as a control subject (GM08429, Coriell Institute) were plated in 6-well plates at 2 × 10^5 cells/well and incubated at 37°C overnight (O/N). The following day, half of the plates were incubated at 40°C for 18 h and all cell lysates were collected in Pierce RIPA Buffer (Thermo Scientific, Cat No. 89900) containing protease inhibitors (Thermo Fisher Scientific, Halt Protease Inhibitor, Cat No. 78430). Cell lysates were sonicated at 40% amplitude for 30 s (Sonics Vibra cell, Model No. VCX130), spun down for 10 min, and quantified using the Pierce BCA Protein Assay Kit (Thermo Scientific, Cat No. 23225). For each sample, 50 μg of protein was run in biological triplicate on a 4%–15% polyacrylamide gel (BioRad, Cat No. 3450027) at 100 V for 2 h 15 min. Proteins were transferred to PVDF membrane (BioRad, Cat No. 162-0177) at 55 V for 65 min and blocked in 3% BSA+ TBST for 1 h at room temperature (RT). RINT1 antibody (Sigma, Cat No. HPA019875) was diluted 1:500 in 3% BSA+ TBST at 4°C O/N. NBAS antibody (Sigma, Cat No. HPA036817) and p31 antibody (Abcam, Cat No. ab111690) were diluted 1:1,000 in 3% BSA+ TBST and incubated at 4°C O/N. Donkey anti-rabbit IgG-HRP (Santa Cruz Biotechnology, Cat No. sc-2313) secondary was incubated at 1:5,000 in 3% BSA+ TBST for 1 h at RT. Membranes were developed with Amersham ECL (GE Healthcare, Cat No. RPN2232) and imaged using LI-COR Odyssey Fc. Membranes were then stripped and re-probed with β-actin antibody (Abcam, Cat No. ab8226) diluted 1:10,000 in 3% BSA+ TBST at 4°C O/N. Goat anti-mouse IgG-HRP (Santa Cruz, Cat No. sc-2005) secondary was diluted 1:5,000 in 3% BSA+ TBST for 1 h at RT. Membranes were again developed with Amersham ECL, imaged on LI-COR, and quantified using LI-COR Image Studio Software.

Golgi and ERGIC Immunofluorescent Imaging

Fibroblasts from probands 1 and 3 as well as a control subject (GM08429, Coriell Institute) were cultured on glass coverslips and incubated at either 37°C or 40°C for 18 h. Cells were fixed in 3% formaldehyde and permeabilized with 0.1% Triton X-100 in dPBS. Fixed cells were stained for 2 h at RT with an antibody against the *cis*-Golgi diluted 1:3,200 (rabbit anti-GM130 [D6B1], Cell Signaling, Cat No. 12480S) or the ERGIC diluted 1:200 (mouse anti-ERGIC-53 [C-6], Santa Cruz Biotechnology, Cat No. sc-365158). The slides were then incubated in a secondary antibody (Alexa Fluor 488 goat anti-rabbit, ThermoFisher, Cat No. A11034, or Alexa Fluor 488 goat anti-mouse ThermoFisher, Cat No. A11001), diluted 1:1,000 for 1 h at 37°C. Nuclei were stained with Hoechst 33342 (Life Technologies, Cat No. H3570). Slides were mounted in ProLong Gold antifade reagent (ThermoFisher, Cat No. P36934) O/N. Representative images were obtained using an LSM780 confocal microscope with a Plan-Apochromat 40X/1.4 oil objective (Zeiss).

LC3 Immunofluorescent Imaging

Fibroblasts from probands 1 and 3 as well as a control subject (GM08429, Coriell Institute) were plated at 1 × 10^6 cells per well on poly-D-lysine (Sigma, Cat No. P6407)-treated glass coverslips and incubated at 37°C O/N. The following day, the cells were treated for 2 h with either 1 μM bafilomycin A1 (Cayman Chemical, Cat# 11038) or DMSO. Cells were then fixed in 4% formaldehyde and permeablized with 0.2% Triton X-100. Cells were stained at 4°C O/N with LC3A/B Ab diluted 1:200 (Cell Signaling, Cat No. 4108S). The slides were then incubated in Alexa Fluor 488 goat anti-rabbit (Invitrogen, Cat No. A11034) diluted 1:500 for 1 h at 37°C. Slides were then mounted in Vectashield with DAPI (Vector Laboratories, Cat No. H-1500) and images were obtained using an LSM780 confocal microscope with a Plan-Apochromat 40×/1.4 oil objective (Zeiss). Five random fields of view were imaged for each of the control, proband 1, and proband 3 cells (±bafilomycin A1). All images were captured using identical acquisition settings on the confocal microscope. Raw .czi images were imported into FIJI (v2.0.0-rc-68/1.52f) for analysis, where each cell was manually segmented and the relative levels of LC3B fluorescence were determined. Background staining values were subtracted to give the final adjusted fluorescence levels per cell.

LC3 Western Blot

Fibroblasts from probands 1 and 3 as well as a control subject (GM08429, Coriell Institute) were plated in 6-well plates at 2 × 10^5 cells/well and incubated at 37°C O/N. The following day, cells were treated for 2 h with 1 μM bafilomycin A1 (Cayman Chemical, Cat No. 11038) or DMSO. Cell lysates were then collected in RIPA buffer + protease inhibitor. Cell lysates were sonicated at 40% amplitude for 30 s, spun down for 10 min, and quantified using the BCA assay. Three independent samples each for control subject, proband 1, and proband 3 cells ± bafilomycin A1 were solubilized in SDS-PAGE loading buffer. Each sample (7.5 μg in 15 μL) was loaded onto a 4%–20% gradient gel and run for 1.5 h at 100 V prior to being transferred onto PVDF. Membranes were probed for β-Actin (Sigma A2066, 1:1,000) or LC3B (Novus NB600-1384, 1:1,000). Secondary antibody was an HRP-conjugated goat anti-rabbit IgG antibody (1:25,000). Chemiluminescence was detected using SuperSignal West Pico Plus ECL substrate (ThermoFisher #34580) for 5 min and imaged using a UVP ChemiDoc-It2 imaging system. Band intensities were quantified using FIJI.

Flow Cytometry

The double-strand break DNA-repair pathway flow assay was performed as described previously[20] on blood lymphocytes from proband 1.

Table 1. Clinical Findings in Individuals with Bi-allelic Alterations in *RINT1* (GenBank: NM_021930)

	Proband 1	Proband 2	Proband 3
Maternal	c.1853_1858del6 (p.Val618_Lys619del)	c.1102G>A (p.Ala368Thr)	c.1109T>C (p.Leu370Pro)
Paternal	c.1333+1G>A (p.?)	c.1333+1G>T (p.?)	c.1333+1G>A (p.?)
Ancestry	mixed European	East Asian	Eastern European
Sex	male	female	female
Birth history			
Gestation	born at 33 6/7 weeks	born at term	born at term
Birth weight	2.53 kg (78th percentile)	3.70 kg (83th percentile)	2,75 kg (5th percentile)
Length	44.5 cm (49th percentile)	54.0 cm (99th percentile)	not available
Head circumference	33.5 cm (92nd percentile)	normal	not available
Neonatal jaundice	yes, peak bilirubin 11.8 mg/dL (direct bilirubin 0.4 mg/dL) at 2 days old; phototherapy	none	none
Dysmorphisms	talipes equinovarus at birth requiring casting	none	none
Newborn screen	borderline elevated methionine, normal with follow-up testing	unremarkable	unremarkable
Weight at last evaluation	normal	normal	normal
Height at last evaluation	<3rd percentile	<3rd percentile	75% percentile
Development	normal	normal	normal
Age at first ALF episode	8 mo	10 mo	3 y
Age at last assessment	died at 3 y 2 mo	8 y 11 mo	7 y 6 mo
Episodes of ALF or acutely elevated transaminases	5	8	4
Age at last episode of ALF/ acutely elevated transaminases	3 y	6 y 8 mo	7 y 3 mo
Acute liver episodes concurrent with illness or fever/total number of episodes	5/5	8/8	4/4
Suspected triggers of episodes	fever or infection	fever with vaccination or infection	illness and fever
Hepatomegaly	+	+	mild (+1–2 cm from RCM)
Splenomegaly	+ (inconsistent)	−	2 cm (in acute setting)
Hepatomegaly between episodes	+	+	none
Laboratory findings during an ALF episode			
Glucose	9 mg/dL (ref: 70–140 mg/dL)	0.2 mmol/L (ref: 3.9–5.8 mmol/L)	1.7 mmol/L
ALT	1,915 U/L (ref: 7–55 U/L)	3,214 U/L (ref: 8–40 U/L)	ca. 2,000 U/L (ref: 0–19 U/L)
AST	5,956 U/L (ref: 8–60 U/L)	1,885 U/L (ref: 10–55 U/L)	ca. 2,000 U/L (ref: 0–33 U/L)
Total bilirubin	7.6 mg/dL (ref: ≤ 1 mg/dL)	3.1 mg/dL (ref: 0.1–1.2 mg/dL)	6.5 mg/dL (ref: 0–0.3 mg/dL)
Direct bilirubin	5.6 mg/dL (ref: 0–0.3 mg/dL)	2.5 mg/dL (ref: 0–0.4 mg/dL)	5.6 mg/dL (ref: 0–0.1 mg/dL)
Prothrombin time	70.6 s (ref: 9.4–12.5 s)	99 s (ref: 11.5–14.9 s)	160 s
INR	7.0 (ref: 0.9–1.1)	5.5 (ref: 0.8–1.2)	>11 (ref: 0.8–1.2)
Highest AST/ALT (U/L) during ALF	5,956/1,915 (1st episode; 8 mo)	3,823/8,318 (3nd episode; 2y2m)	>16,646/8,429 IU/L

(Continued on next page)

Table 1. Continued

	Proband 1	Proband 2	Proband 3
Lowest AST/ALT (U/L) between episodes	122/282 (2 y)	25/44 (6 y 5 mo) completely normalized by 8 yo	normal
Age at liver biopsy	10 mo 8 d	1 y 9 mo	7 y 4 mo
Liver biopsy findings			
Steatosis	+	+	−
Fibrosis	+	−	−
Increase in Kupffer cells	−	−	+
AST/ALT (U/L) at liver biopsy	458/431 (12 days prior to biopsy)	28/43 (2 days prior to biopsy)	14/30 (2 days prior liver biopsy)
Retroperitoneal ultrasound	normal	normal	hyperechoic cortex of both kidneys
Echocardiogram	normal	normal	satisfactory biventricular function; minimal aortic insufficiency; elevated R side pressures
Skeletal findings			
Hypoplastic vertebrae	+	+	+
Beaked vertebrae	+	+	+
Irregular vertebrae	+	+	+
Platyspondyly	+	−	−
Acetabular abnormalities	+	+	−
Abnormal femoral head epiphysis	+	+	+

Results

Clinical Findings

Three unrelated individuals with RALF concurrent with fever and/or infection and skeletal abnormalities were identified and suspected as having an underlying genetic etiology of their disease. Clinical findings are summarized in Table 1 and detailed clinical histories of each individual can be found in the Supplemental Note. All had unremarkable births, neonatal periods, and family histories. Two of three affected children have short stature, but all have had otherwise normal development and cognition. Onset of ALF ranged from 8 months to 3 years of age. Episodic liver dysfunction was significant with hyperammonemia and coagulopathy that required supportive care. Probands 1 and 2 had abnormal liver transaminase levels that did not recover to normal between early childhood episodes. However, the liver enzymes of proband 2 did eventually normalize by age 7 years. Proband 3 has had normal liver transaminases between episodes since disease onset; she recently underwent liver transplantation at the age of 8 years. Proband 1 died of acute respiratory failure at 3 years of age.

Liver biopsies failed to show any specific abnormalities by light or electron microscopy (Figure 1), but steatosis (probands 1 and 2) and bridging fibrosis (proband 1) were noted. There was also a mild increase in Kupffer cells indicative of resolving hepatocellular injury and focal hepatocellular cholestasis (proband 3). No ultrastructural changes were identified, but numerous lipid droplets were seen in the hepatocytes and the Golgi could not be clearly observed.

Based on skeletal changes observed in some individuals with NBAS deficiency, skeletal surveys were performed for probands 1 and 2, and skeletal imaging for proband 3, with representative images shown in Figure 2. All three individuals demonstrate vertebral body abnormalities including anterior beaking and irregularity, with at least one hypoplastic vertebral body. Proband 1 also has platyspondyly and probands 1 and 2 have acetabular abnormalities. All three children have irregularity of the femoral head epiphyses with asymmetry or decreased spherical contour. These findings are similar in appearance to the skeletal phenotypes observed in individuals with mucopolysaccharidoses and other lysosomal storage diseases, often referred to as dysostosis multiplex. The dense metaphyseal bands seen in proband 1 are nonspecific, can be seen with multiple systemic pathologies, and could be due to his iron-deficiency anemia.

RINT1 interacts with RAD50, and N-terminally truncated RINT1 exhibited aberrant radiation-induced G2-M checkpoint control, suggesting that it may have a role in cellular regulation after DNA damage.[21] The DNA repair pathway was assessed[20] in proband 1 using blood cells and no detectable deficiencies in the radiation-induced double-strand break repair pathway were found (Figure S2).
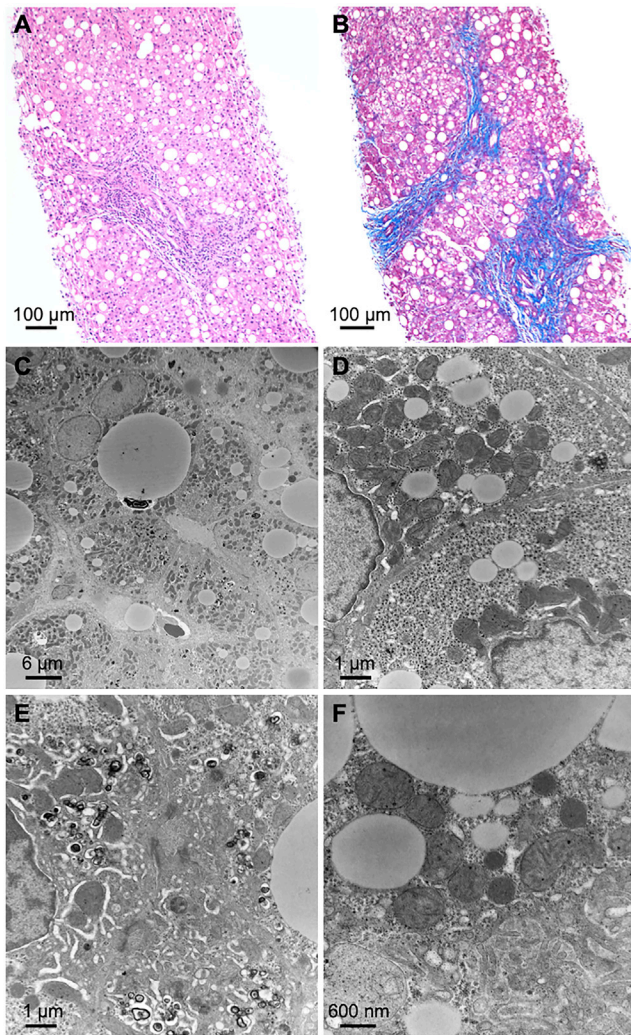
Figure 1. Liver Biopsies from Proband 1 Show Non-specific Findings Consistent with Liver Damage
(A) H&E shows moderate macrovesicular steatosis (200× magnification).
(B) Trichrome stain shows bridging fibrosis (100× magnification).
(C) Numerous lipid droplets are present in hepatocytes (HV = 80.0 kV; 2,100× direct magnification).
(D) Glycogen contents are in the normal range and there are no visible abnormalities in the endoplasmic reticulum (HV = 80.0 kV; 11,000× direct magnification).
(E) The bile canaliculus (center) is normal. Electron dense material consistent with biliary material is seen in the hepatocellular cytoplasm surrounding the bile canaliculus (HV = 80.0 kV; 11,000× direct magnification).
(F) There are no abnormalities of mitochondria and peroxisomes are present (HV = 80.0 kV; 21,000× direct magnification).

Bi-allelic Variants in *RINT1* Identified by Whole-Exome Sequencing

WES revealed compound heterozygous variants in *RINT1* in each of the three affected individuals (Table 2 and Figure 3). Interestingly, a single-nucleotide variant at the same canonical exon 9 splice donor site (c.1333+1G>A or c.1333+1G>T), predicted to abolish the exon 9 splice donor, was found in each proband.

The c.1333+1G>A variant has been previously reported in the heterozygous state in one individual in a cohort with early-onset breast cancer.[22] The other allele in probands 2 and 3 harbored missense alterations (c.1102G>A [p.Ala368Thr] and c.1109C>T [p.Leu370Pro]) and in proband 1 a two-residue deletion (c.1853_1858del [p.Val618_Lys619del]). Sanger sequencing of the parents determined phase and inheritance of each variant in family 2 (Figure S1). All variants are either rare or absent in gnomAD (v.2.1),[23] which reported no homozygous variants at these positions (Table 2). The missense and in-frame deletion variants affect conserved residues in the protein and are predicted to be damaging (Figure 3).

Variant at Splice Position Leads to Exon Skipping and Nonsense-Mediated Decay

All three probands have a canonical splice variant at the same genomic position, and whole transcriptome sequencing of cultured fibroblasts from proband 1 was used to characterize the splicing impact. We observed 3 reads (3.3% of junction reads between exons 8, 9, and 10) supporting splicing from exon 8 to exon 10 and skipping exon 9, 40 reads supporting canonical splicing from exon 8 to 9, and 49 supporting canonical splicing from exon 9 to 10 (Figure 4). Treatment of fibroblasts with puromycin to block protein translation and nonsense-mediated decay (NMD) recovered additional reads supporting exon 9 skipping. We observed 31 reads (23.0% of junction reads between exons 8, 9, and 10) supporting exon 9 skipping, 51 reads supporting canonical splicing from exon 8 to 9, and 53 supporting canonical splicing from exon 9 to 10. These data indicate that the splice variant at c.1333+1 causes exon 9 skipping (deletion of residues 370–444) and a frameshift leading to a premature stop codon in exon 10 that is predicted to undergo NMD. We did not see any evidence of an alternative splice donor being used in the RNA sequencing data and we interpret these splice variants as loss-of-function (LoF) alterations. These data are consistent with RT-PCR assays showing exon 9 skipping in a carrier of the c.1333+1G>A in a breast cancer cohort.[22]

Protein Studies

Individuals with pathogenic bi-allelic *NBAS* alterations were shown previously to have a decreased level of NBAS protein in dermal fibroblasts,[3,4] which was further decreased when cells were cultured at 40°C, relative to control fibroblasts.[4] This may suggest a thermal instability of the NBAS protein in affected individuals. To determine whether bi-allelic *RINT1* alterations have a similar effect, we measured RINT1 protein levels in primary dermal fibroblasts from probands 1 and 3. The fibroblasts from both individuals showed a decrease in RINT1 protein compared to control fibroblasts (Figure 5A, single factor effect; $F_{2,12} = 98.17$, p = 3.65e−8, 2-way ANOVA). There was no significant effect of temperature (37°C versus
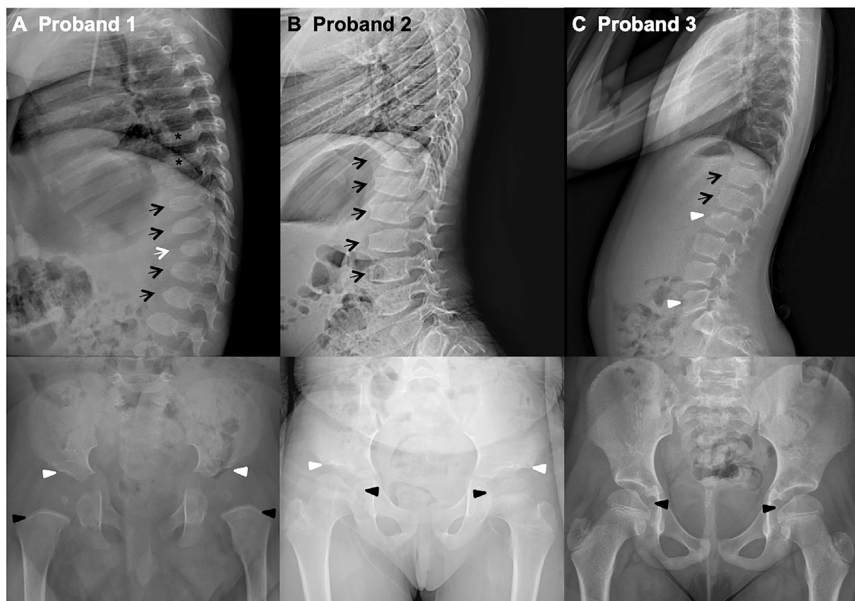
Figure 2. Radiographic Skeletal Findings
(A) Proband 1: 15-month-old male with beaking of several lower thoracic and upper lumbar spine vertebrae (black arrows) with a hypoplastic T12 vertebra (white arrow) and platyspondyly of the thoracic vertebrae (asterisks). The acetabula are mildly shallow (white arrowheads) with an asymmetrically small right femoral head epiphysis. Dense metaphyseal bands were also noted in the long bones (black arrowheads).
(B) Proband 2: 7-year-old female. Lateral radiograph of the spine shows anterior beaking of lower thoracic and lumbar vertebra (black arrows). Frontal pelvic radiograph shows mild irregularity of the acetabular rims (white arrowheads), as well as decreased spherical contour of the femoral head epiphyses (black arrowheads).
(C) Proband 3: 8-year-old female. Lateral radiograph of the spine shows findings of mild anterior vertebral irregularity and beaking of lower thoracic and upper lumbar vertebrae (black arrows), with mild hypoplasia of the anterior aspects of L2 and L5 vertebrae (white arrowheads). Frontal pelvic radiograph shows the femoral head epiphyses to be flattened medially (black arrowheads) with decreased spherical contour, which may be due to an unusually large fovea capitis.

$40°C$) (single factor effect; $F_{1,12} = 4.73$, p = 0.05); however, a trend toward further decrease in RINT1 protein at $40°C$ was observed. NBAS and p31 (*USE1* gene product) protein levels in the fibroblast cultures were not significantly different from control fibroblasts (Figures 5B and 5C).

Previous cell-based studies have shown depletion of RINT1 leads to abnormal Golgi structure[8] and vesicle-tethering defects were observed in NBAS-deficient individuals.[4] Fibroblasts from probands 1 and 3 in this study show an expanded Golgi network by GM130 immunofluorescence and those from proband 1 also demonstrate Golgi fragmentation after culture at $40°C$, not seen in control or proband 3 cells (Figure 6A). Immunofluorescent staining of the ER-Golgi intermediate compartment (ERGIC53) suggests a more diffuse and expanded ERGIC as well (Figure 6B), which may be consistent with vesicles having inefficient trafficking and docking to the ER in retrograde vesicle transport.

RINT1 deficiency has been previously associated with defective autophagy in conditional KO mouse neurons.[24] Consistent with these data, we show that fibroblasts from probands 1 and 3 have statistically significant increases in cytoplasmic LC3 by immunofluorescence (IF) and LC3-II by western blot (p < 0.0001 and p = 0.0059 by IF; p = 0.007 and p = 0.029 by WB, respectively), with proband 1 showing a larger magnitude of difference from control than proband 3 (Figures 6C and 6D). The increased LC3 staining was not further exacerbated by treatment with bafilomycin A1, an inhibitor of autophagosome-lysosome fusion, suggesting a decrease in autophagosome clearance in the fibroblasts of these individuals.

Discussion

WES of three unrelated children with RALF and skeletal anomalies enabled identification of bi-allelic alterations in *RINT1* as the cause of disease. The consistent clinical findings include onset at 3 years of age or younger of RALF concurrent with fever/infection and nonspecific findings of liver injury on biopsy. Liver function may fully or partially recover to normal function between acute episodes. Vertebral body abnormalities including anterior beaking, irregularity, and hypoplasia were consistently observed with some irregularity of the femoral head epiphyses with or without acetabular abnormalities. Compound heterozygous *RINT1* variants including a missense or in-frame deletion on one allele and a variant affecting the exon 9 splice donor on the other allele were identified in each affected individual.

Whole-transcriptome sequencing of fibroblast RNA demonstrated exon 9 skipping as a result of the single-nucleotide variant at c.1333+1 likely causing the transcript to undergo NMD and contributing to the decreased RINT1 protein levels observed. The mechanism by which the missense and in-frame deletion alleles contribute to reduced RINT1 protein levels is unclear. Homozygous loss of *rint1* in mice is early embryonic lethal[8] and likely not compatible with life in humans, but haploinsufficiency does not cause a phenotype. Therefore, we hypothesize the missense and in-frame deletion alleles are hypomorphic and cause disease when in *trans* with a LoF allele. Whether they also would cause disease in the homozygous state is undetermined.

The clinical overlap between the individuals we describe with RINT1 deficiency and the cohort with bi-allelic

Table 2. *RINT1* Bi-allelic Variants (GenBank: NM_021930.5)

Proband (Inher.)	Nucleotide	Protein	Gene Location	gnomAD AF	*in silico* predictions (SIFT; PolyPhen; Mutation Taster; M-CAP; PredictSNP2)
Pr 2 (mat)	c.1102G>A	p.Ala368Thr	exon 8	2/250760 (no hom)	tolerated; probably damaging; disease causing; possibly pathogenic; deleterious
Pr 3 (mat)	c.1109T>C	p.Leu370Pro	exon 9	not reported	deleterious; probably damaging; disease causing; possibly pathogenic; deleterious
Pr 1 (pat) & Pr 3 (pat)	c.1333+1G>A	p.?	intron 9	13/251316 (no hom)	N/A
Pr 2 (pat)	c.1333+1G>T	p.?	intron 9	not reported	N/A
Pr 1 (mat)	c.1853_1858del6	p.Val618_Lys619del	exon 12	not reported	N/A

Abbreviations: Inher., inheritance; AF, allele frequency; Pr, proband; mat, maternal; pat, paternal; hom, homozygous; N/A, not applicable.

pathogenic variations in *NBAS* is striking. Both disorders present with fever- or illness-dependent episodes of RALF that improved with age with the first episode of ALF occurring in infancy or early childhood (8 months to 3 years). The oldest first episode of *RINT1*-associated RALF did occur 1 year later than the oldest child with *NBAS*-associated RALF. Both *NBAS*- and *RINT1*-associated ALF episodes occur with vomiting and impaired mental status prior to presentation. The ALF episodes in both disorders are associated with elevated AST and ALT, severe coagulopathy, and hyperbilirubinemia. Some individuals also experienced hypoglycemia, hyperammonemia, and hepatic encephalopathy, but hypoglycemia is thought to have been prevented in subsequent proband 1 episodes due to early intervention with fever control and glucose administration, as has been described for individuals with NBAS deficiency.[4] Liver function, however, did not always quickly recover as typically seen with *NBAS*-associated RALF in the cohort described by Staufner et al.,[4] and liver biopsies also differed. NBAS deficiency was associated with microvesicular steatosis without fibrosis and ER were usually enlarged. Bi-allelic *RINT1* alterations were associated with macrovesicular steatosis in two individuals, bridging fibrosis seen in one, and normal electron microscopy. Looking at all published *NBAS*-affected case subjects and our own cohort, there are individuals with normalization of liver enzymes in the interval but as well some with continuously elevated liver function tests similar to the individuals with RINT1 deficiency. Of special interest will be the further course of proband 3 who recently underwent liver transplantation.

The *RINT1*- and *NBAS*-associated RALF is different from other hepatopathy-associated syndromes caused by intracellular trafficking defects. For example, in individuals with hepatopathy associated with mutations in *ATP6AP1* (MIM: 300972), the phenotypic spectrum ranges from mild transaminitis to cirrhosis and end-stage liver failure without the consistent finding of recurrent episodes associated with fever or illness.[25] In individuals with a congenital disorder of glycosylation (CDG) caused by *CCDC115* (MIM: 613734), the hepatic presentation ranges from hepatosplenomegaly at birth to elevated aminotransfer-ases detected as late as age 20, incidentally.[26] These presentations are in contrast with the *RINT1* phenotype, as hepatic changes are not expected at birth but rather after illness in infants who are affected. Additionally, although we have not fully defined the clinical spectrum of *RINT1*-associated RALF, we have not yet seen more subtle adult-onset hepatic presentations as sometimes seen with the CDG-associated hepatopathies.

Outside of the liver findings, the skeletal phenotypes observed in individuals with bi-allelic pathogenic *RINT1* variants are distinct from those in individuals with NBAS deficiency and are reminiscent of a lysosomal storage disorder. In particular, the lower thoracic and lumbar vertebral beaking have not been reported in NBAS deficiency to date. Within the phenotypic spectrum of NBAS deficiency, some individuals present with skeletal abnormalities that have been characterized as atypical osteogenesis imperfecta with bone fragility including fractures, slender tubular bones, osteopenia,[27,28] SOPH syndrome (MIM: 614800),[29] and acrofrontofacionasal dysostosis type 1 (MIM: 201180).[30] The differences in skeletal phenotypes suggest unique pathobiological mechanisms of disease in RINT1-deficient individuals from that of NBAS deficiency at least as it pertains to bone development.

RINT1 and NBAS, as part of the NRZ complex, do play a role in docking and fusion of transport vesicles in the *trans*-Golgi network as a component of an endoplasmic reticulum (ER) tethering complex which binds target SNAREs at the ER.[31] The NRZ complex is a critical component in Golgi-to-ER retrograde transport of COPI-coated vesicles in conjunction with ER SNAREs.[32–34] Retrograde transport is important for membrane recycling for organelle homeostasis and returning proteins to the ER that may have been inappropriately delivered. The cooperative roles of RINT1 and NBAS in the NRZ complex suggest similar disease etiology for the hepatic phenotype observed in RINT1- and NBAS-deficient individuals. Mechanistically, it is hypothesized that NBAS deficiency causes liver failure during fever/infection secondary to ER-stress-induced hepatocyte apoptosis.[4] Primary fibroblasts from individuals with pathogenic bi-allelic *NBAS* alterations demonstrated decreased levels of NBAS and p31 in normal culture conditions[3]
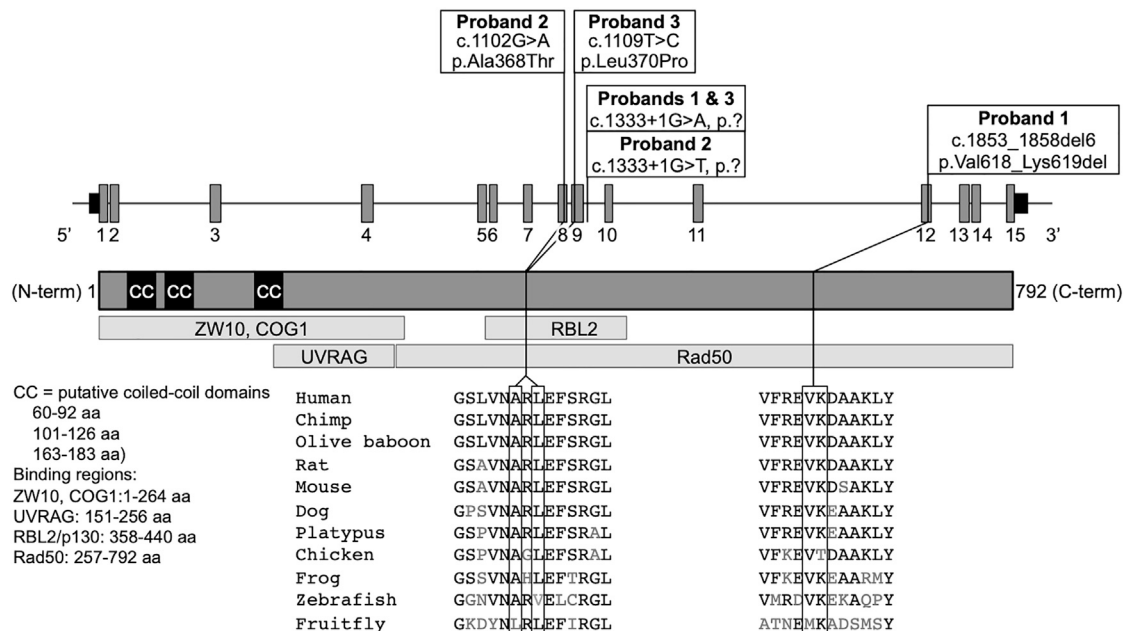
Figure 3. Bi-allelic *RINT1* Variants
Gene (GenBank: NM_021930) and protein schematics showing the location of the variants identified in RINT1 and the species conservation of the affected residues of the missense and in-frame deletion alterations. Introns are not to scale.

with further decrease caused by increased temperature to mimic liver crises occurring with illness.[4] Knockdown studies of *NBAS* also showed reduced p31 levels indicating NBAS is required for p31 stability.[32] Furthermore, dermal fibroblasts from affected individuals, after membrane permeabilization, demonstrated reduced presence of *cis*-Golgi and ER-Golgi intermediate compartment, suggesting defective tethering of the vesicles of these compartments.[4] The decreased amount of p31 could suggest the entire complex, including RINT1, is temperature sensitive, fitting with the phenotype of the affected children described herein. Haack et al.[3] hypothesized that the initial perturbation leading to liver failure during fever/infection in *NBAS*-associated RALF might be either a catabolic state with high-energy demand or the increased temperature itself.

Using primary fibroblast cultures, we show that bi-allelic pathogenic *RINT1* alterations lead to a significant decrease in RINT1 protein. These cells also show a trend (not statistically significant) toward even less protein with an increase in temperature. This experiment was conducted with biological triplicates, but detection of decreased levels from an already reduced level of protein is challenging. No significant differences are seen in NBAS or p31 levels, however, suggesting that the deficiency or instability of RINT1 does not affect NBAS and p31 protein levels. Interestingly, we observe a slightly smaller second band for p31 in fibroblasts from proband 1 for which the significance is unclear.

Phenotypically, we show dermal fibroblasts from individuals with *RINT1*-associated RALF demonstrate abnormal Golgi morphology that is consistent with what has been shown previously in various cell models of RINT1 deficiency.[8,24,31,35–37] The Golgi in these fibroblasts appear expanded and more diffuse. Proband 1 has a fragmented appearance to the Golgi network after culture at increased temperature that is not seen in proband 3 or the control subject, suggesting a unique or more severe functional deficit imparted by the in-frame two-residue deletion present in this individual.

Recently published work highlights the additional role of the NRZ complex in the secretory pathway interacting with TANGO1 (*MIA3* [MIM: 613455]) and cTAGE5 (*MIA2* [MIM: 602132]) at the ER exit site; loss of RINT1 or NBAS in cells impairs the anterograde transport of collagen VII.[38] If this process holds true for other collagens, such interactions could be relevant to the development of the skeletal phenotypes in both *RINT1*- and *NBAS*-related diseases. Additionally, in mouse neurons with RINT1 loss, inhibition of autophagosome clearance and increased cell death was observed.[24] Impaired autophagic flux was also observed in the fibroblast studies described, here, that may be contributing to the clinical presentation. The IF imaging and WB studies of LC3 in skin-derived cells suggest an impairment of autophagosome clearance. Importantly, this experiment reflects basal autophagy levels in these cells, which correlates to the modest increase in autophagosome accumulation seen in the control cells treated with bafilomycin A1. Whether loss or dysfunction of RINT1 causes impaired autophagic flux via inefficient or aberrant intracellular vesicular trafficking remains unclear and warrants further investigation.

The Golgi-to-ER retrograde transport protein complex includes UVRAG (MIM: 602493) that contributes both to
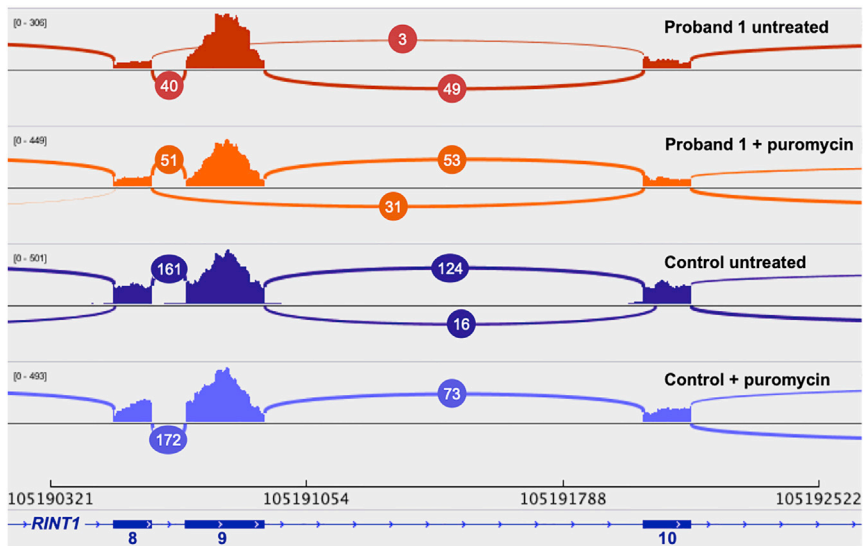
Figure 4. RNA Sequencing from Fibroblasts Reveals Skipping of Exon 9 of *RINT1*
Sashimi plot representing RNA sequencing reads supporting splicing junctions of exons 8, 9, and 10 of *RINT1* (GenBank: NM_021930) from fibroblast cultures from proband 1 and a control (±puromycin). The junction reads from proband 1 reveal skipping of exon 9 with recovery of additional reads supporting exon 9 skipping with puromycin treatment. No exon 9 skipping was observed in the control.

ER-docking within retrograde transport by binding to RINT1 and to autophagy initiation, playing a role in the switching between these processes.[39] During stimulation of autophagy, UVRAG dissociates from RINT1 attenuating Golgi-to-ER retrograde transport, and associates with BECN1 (MIM: 604378).[39] Furthermore, the biogenesis of autophagic vacuoles is a trafficking pathway that delivers cargo to the lysosomes[40] and involves COPI-coated vesicles recognized by the NRZ complex.[41] Depletion of COPI proteins in yeast causes LC3-marked autophagic vesicles to accumulate and autophagy to be inhibited.[41] It is reasonable to consider that RINT1 dysfunction may lead to aberrant autophagy either through deregulation of autophagy induction or through disrupted vesicle trafficking.

Aberrant autophagy may contribute to skeletal and liver phenotypes seen in individuals with *RINT1*-associated disease. Autophagy is a necessary component to post-natal bone growth[42] and has also been implicated in liver disease.[43–45] Autophagy induction in growth plate chondrocytes regulates the secretion of type II collagen (Col2), the primary component of cartilage matrix. Mouse and human cellular models of bone development in lysosomal storage diseases show that defects in autophagy initiation or autophagosome clearance lead to type II procollagen accumulation, increased mTORC1 activity, and significantly decreased autophagic vesicle-lysosome fusion (autophagosome maturation) due to mTORC1 inhibition of UVRAG.[42,46] Similarly, impaired autophagy in the liver is implicated in the pathophysiology of non-alcoholic fatty liver disease that leads to steatosis, fibrosis, and liver injury.[43,45] This also involves the accumulation of autophagosomes resulting from decreased clearance[44] as seen in this study, the degree of which correlates with disease severity.[43,45] How RINT1 and the NRZ complex affects or is affected by mTORC1-mediated metabolic regulation will need to be studied further to better understand the acute liver crises and bone development abnormalities seen in individuals with pathogenic bi-allelic *RINT1* alterations.
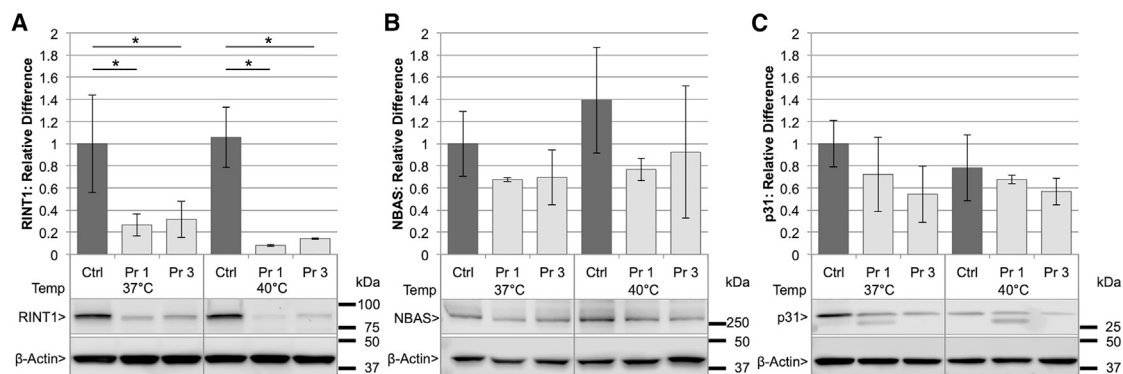

Figure 5. Fibroblasts Demonstrate Decreased RINT1 Protein, but Not NBAS or p31
(A) There is a significant difference in RINT1 protein levels among the genetic variants (control [Ctrl], proband 1 [Pr 1], or proband 3 [Pr 3]) (single factor effect; $F_{2,12} = 98.17$, $p = 3.65e-8$). There is no significant effect of temperature (37°C versus 40°C) (single factor effect; $F_{1,12} = 4.73$, $p = 0.05$). There is no significant effect on RINT1 protein levels of the interaction between the genetic variants (Ctrl, Pr 1, or Pr 3) and temperature (37°C or 40°C) ($F_{2,12} = 1.30$, $p = 0.31$).
(B and C) No statistically significant reduction in NBAS protein (B) or p31 protein (C) levels compared to control were observed. 2-way analysis of variance (2-way ANOVA) from three independent experiments each. *$p < 0.05$.
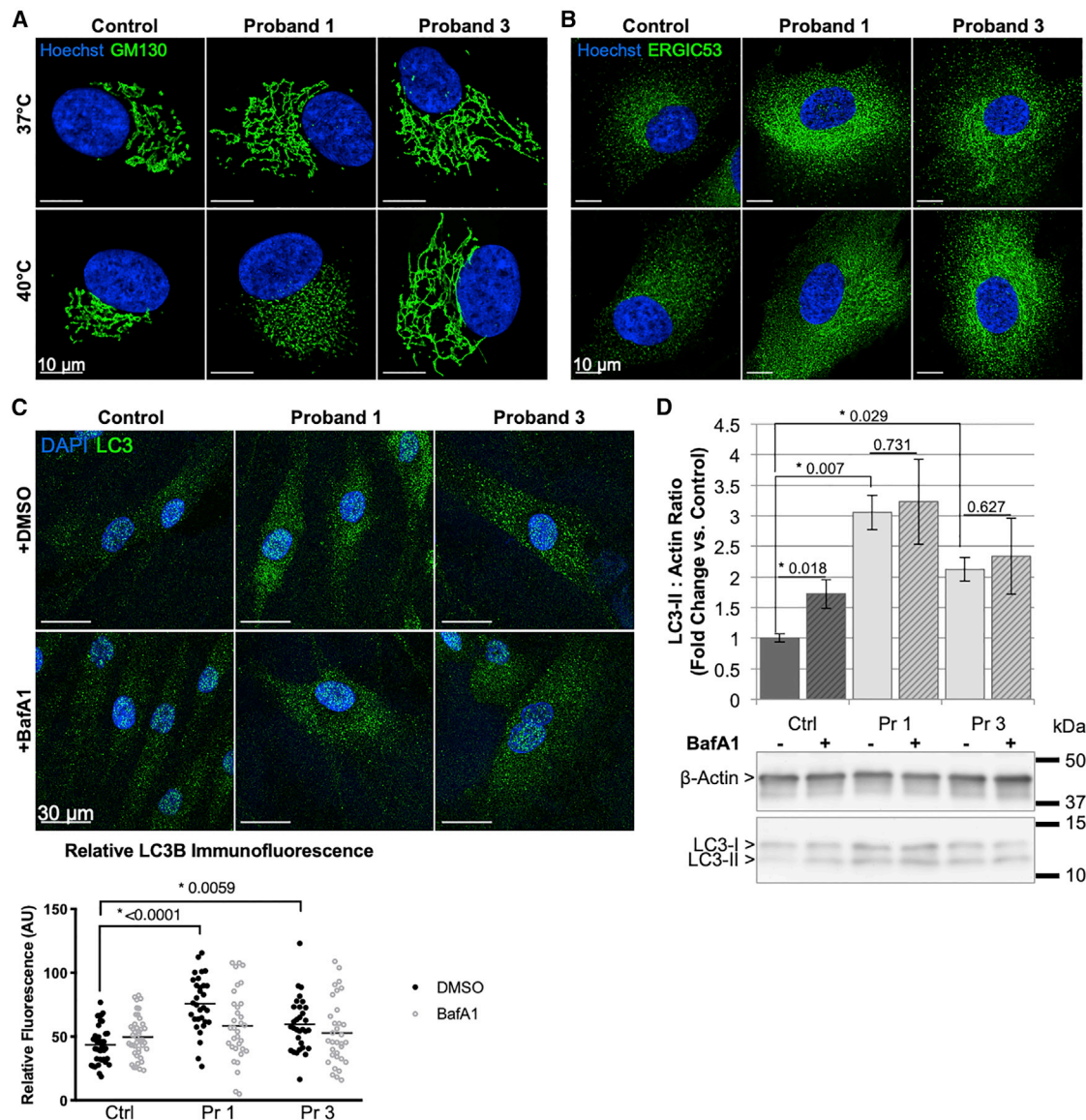
Figure 6. Fibroblasts Have Abnormal Golgi Morphology and Impaired Autophagic Flux

(A and B) Fibroblasts from affected individuals and a control were cultured at 37°C or 40°C and show (A) an expanded Golgi network with proband 1 also showing fragmentation of the Golgi at 40°C, compared to control by GM130, and (B) possible expansion of the ER-Golgi intermediate compartment (ERGIC) by ERGIC53.

(C) Fibroblasts cultured with and without bafilomycin A1 (BafA1) show increased LC3 by immunofluorescent imaging that was not further increased by bafilomycin A1 treatment compared to control.

(D) Whole-cell lysates from each proband show an increase in LC3-II/Actin ratio compared to control. The LC3-II/Actin ratio in control cells was increased with bafilomycin A1 treatment, but remained unchanged in probands 1 and 3.

Ctrl, control; Pr, proband; bars represent mean ± standard deviation for three independent experiments. Two-tailed paired t test.

Other functions of RINT1 include maintaining centrosome integrity and *RINT1* has been associated with intermediate levels of breast cancer risk and Lynch syndrome-spectrum cancers based on enrichment of heterozygous variants in a disease cohort and a heterozygous mouse model.[8,22] However, there is no clear mechanism for these effects and conflicting findings were observed in later studies.[47,48] Due to the RINT1 and RAD50 interaction, we evaluated the double-strand break DNA-repair pathway using flow cytometry[20] and observed a normal DNA-repair pathway response in lymphocytes. Therefore,

the observed compound heterozygous variants in *RINT1* do not appear to be interfering with ATM (MIM: 607585) or H2AX (*H2AFX* [MIM: 601772]) phosphorylation (γH2AX) in lymphocytes, suggesting that this pathway of DNA repair seems to be unaffected in lymphocytes.

In summary, we describe three unrelated children with RALF and skeletal abnormalities who have compound heterozygous alterations in *RINT1* leading to RINT1 deficiency, abnormal Golgi morphology, and impaired autophagic flux. We propose that *RINT1* bi-allelic pathogenic variations cause a previously unrecognized disorder that

has features of RALF similar to NBAS-deficient individuals with unique skeletal features.

Accession Numbers

The accession numbers for the following sequence variants reported in this paper are as follows. GenBank: NM_021930.5 (RINT1): c.1102G>A (p.Ala368Thr) – LOVD Variant ID: 0000443410; GenBank: NM_021930.5 (RINT1): c.1109T>C (p.Leu370Pro) – ClinVar: SCV000863784; GenBank: NM_021930.5 (RINT1): c.1333+1G>A (p.?) – ClinVar: SCV000782632.1 and SCV000864213; GenBank: NM_021930.5 (RINT1): c.1333+1G>T (p.?) – LOVD Variant ID: 0000443411; GenBank: NM_021930.5 (RINT1): c.1853_1858del (p.Val618_Lys619del) – ClinVar: SCV000782631.1.

Supplemental Data

Supplemental Data can be found online at https://doi.org/10.1016/j.ajhg.2019.05.011.

Web Resources

FastQC, http://www.bioinformatics.babraham.ac.uk/projects/fastqc
GenBank, https://www.ncbi.nlm.nih.gov/genbank/
gnomAD Browser, https://www.gnomad.broadinstitute.org/
OMIM, https://www.omim.org/

References

1. Squires, R.H., Jr., Shneider, B.L., Bucuvalas, J., Alonso, E., Sokol, R.J., Narkewicz, M.R., Dhawan, A., Rosenthal, P., Rodriguez-Baez, N., Murray, K.F., et al. (2006). Acute liver failure in children: the first 348 patients in the pediatric acute liver failure study group. J. Pediatr. 148, 652–658.

2. Narkewicz, M.R., Dell Olio, D., Karpen, S.J., Murray, K.F., Schwarz, K., Yazigi, N., Zhang, S., Belle, S.H., Squires, R.H.; and Pediatric Acute Liver Failure Study Group (2009). Pattern of diagnostic evaluation for the causes of pediatric acute liver failure: an opportunity for quality improvement. J. Pediatr. 155, 801–806.e1.

3. Haack, T.B., Staufner, C., Köpke, M.G., Straub, B.K., Kölker, S., Thiel, C., Freisinger, P., Baric, I., McKiernan, P.J., Dikow, N., et al. (2015). Biallelic Mutations in NBAS Cause Recurrent Acute Liver Failure with Onset in Infancy. Am. J. Hum. Genet. 97, 163–169.

4. Staufner, C., Haack, T.B., Köpke, M.G., Straub, B.K., Kölker, S., Thiel, C., Freisinger, P., Baric, I., McKiernan, P.J., Dikow, N., et al. (2016). Recurrent acute liver failure due to NBAS deficiency: phenotypic spectrum, disease mechanisms, and therapeutic concepts. J. Inherit. Metab. Dis. 39, 3–16.

5. Regateiro, F.S., Belkaya, S., Neves, N., Ferreira, S., Silvestre, P., Lemos, S., Venâncio, M., Casanova, J.L., Gonçalves, I., Jouanguy, E., and Diogo, L. (2017). Recurrent elevated liver transaminases and acute liver failure in two siblings with novel bi-allelic mutations of NBAS. Eur. J. Med. Genet. 60, 426–432.

6. Li, J.Q., Qiu, Y.L., Gong, J.Y., Dou, L.M., Lu, Y., Knisely, A.S., Zhang, M.H., Luan, W.S., and Wang, J.S. (2017). Novel NBAS mutations and fever-related recurrent acute liver failure in Chinese children: a retrospective study. BMC Gastroenterol. 17, 77.

7. Calvo, P.L., Tandoi, F., Haak, T.B., Brunati, A., Pinon, M., Olio, D.D., Romagnoli, R., and Spada, M. (2017). NBAS mutations cause acute liver failure: when acetaminophen is not a culprit. Ital. J. Pediatr. 43, 88.

8. Lin, X., Liu, C.C., Gao, Q., Zhang, X., Wu, G., and Lee, W.H. (2007). RINT-1 serves as a tumor suppressor and maintains Golgi dynamics and centrosome integrity for cell survival. Mol. Cell. Biol. 27, 4905–4916.

9. McKenna, A., Hanna, M., Banks, E., Sivachenko, A., Cibulskis, K., Kernytsky, A., Garimella, K., Altshuler, D., Gabriel, S., Daly, M., and DePristo, M.A. (2010). The Genome Analysis Toolkit: a MapReduce framework for analyzing next-generation DNA sequencing data. Genome Res. 20, 1297–1303.

10. Kocher, J.P., Quest, D.J., Duffy, P., Meiners, M.A., Moore, R.M., Rider, D., Hossain, A., Hart, S.N., and Dinu, V. (2014). The Biological Reference Repository (BioR): a rapid and flexible system for genomics annotation. Bioinformatics 30, 1920–1922.

11. Qiu, Y.L., Gong, J.Y., Feng, J.Y., Wang, R.X., Han, J., Liu, T., Lu, Y., Li, L.T., Zhang, M.H., Sheps, J.A., et al. (2017). Defects in myosin VB are associated with a spectrum of previously undiagnosed low γ-glutamyltransferase cholestasis. Hepatology 65, 1655–1669.

12. Lenz, D., McClean, P., Kansu, A., Bonnen, P.E., Ranucci, G., Thiel, C., Straub, B.K., Harting, I., Alhaddad, B., Dimitrov, B., et al. (2018). SCYL1 variants cause a syndrome with low γ-glutamyl-transferase cholestasis, acute liver failure, and neurodegeneration (CALFAN). Genet. Med. 20, 1255–1265.

13. Li, H., and Durbin, R. (2009). Fast and accurate short read alignment with Burrows-Wheeler transform. Bioinformatics 25, 1754–1760.

14. Li, H., Handsaker, B., Wysoker, A., Fennell, T., Ruan, J., Homer, N., Marth, G., Abecasis, G., Durbin, R.; and 1000 Genome Project Data Processing Subgroup (2009). The Sequence Alignment/Map format and SAMtools. Bioinformatics 25, 2078–2079.

15. Kalari, K.R., Nair, A.A., Bhavsar, J.D., O'Brien, D.R., Davila, J.I., Bockol, M.A., Nie, J., Tang, X., Baheti, S., Doughty, J.B., et al. (2014). MAP-RSeq: Mayo Analysis Pipeline for RNA sequencing. BMC Bioinformatics 15, 224.

16. Kim, D., Pertea, G., Trapnell, C., Pimentel, H., Kelley, R., and Salzberg, S.L. (2013). TopHat2: accurate alignment of transcriptomes in the presence of insertions, deletions and gene fusions. Genome Biol. *14*, R36.

17. Langmead, B. (2010). Aligning short sequencing reads with Bowtie. Curr. Protoc. Bioinformatics *Chapter 11*, 7.

18. Anders, S., Pyl, P.T., and Huber, W. (2015). HTSeq–a Python framework to work with high-throughput sequencing data. Bioinformatics *31*, 166–169.

19. Quinlan, A.R. (2014). Bedtools: the swiss-army tool for genome feature analysis. Curr. Protoc. Bioinformatics *47*, 1–34.

20. Cousin, M.A., Smith, M.J., Sigafoos, A.N., Jin, J.J., Murphree, M.I., Boczek, N.J., Blackburn, P.R., Oliver, G.R., Aleff, R.A., Clark, K.J., et al. (2018). Utility of DNA, RNA, Protein, and Functional Approaches to Solve Cryptic Immunodeficiencies. J. Clin. Immunol. *38*, 307–319.

21. Xiao, J., Liu, C.C., Chen, P.L., and Lee, W.H. (2001). RINT-1, a novel Rad50-interacting protein, participates in radiation-induced G(2)/M checkpoint control. J. Biol. Chem. *276*, 6105–6111.

22. Park, D.J., Tao, K., Le Calvez-Kelm, F., Nguyen-Dumont, T., Robinot, N., Hammet, F., Odefrey, F., Tsimiklis, H., Teo, Z.L., Thingholm, L.B., et al. (2014). Rare mutations in RINT1 predispose carriers to breast and Lynch syndrome-spectrum cancers. Cancer Discov. *4*, 804–815.

23. Lek, M., Karczewski, K.J., Minikel, E.V., Samocha, K.E., Banks, E., Fennell, T., O'Donnell-Luria, A.H., Ware, J.S., Hill, A.J., Cummings, B.B., et al.; Exome Aggregation Consortium (2016). Analysis of protein-coding genetic variation in 60,706 humans. Nature *536*, 285–291.

24. Grigaravicius, P., Kaminska, E., Hübner, C.A., McKinnon, P.J., von Deimling, A., and Frappart, P.O. (2016). Rint1 inactivation triggers genomic instability, ER stress and autophagy inhibition in the brain. Cell Death Differ. *23*, 454–468.

25. Jansen, E.J., Timal, S., Ryan, M., Ashikov, A., van Scherpenzeel, M., Graham, L.A., Mandel, H., Hoischen, A., Iancu, T.C., Raymond, K., et al. (2016). ATP6AP1 deficiency causes an immunodeficiency with hepatopathy, cognitive impairment and abnormal protein glycosylation. Nat. Commun. *7*, 11600.

26. Girard, M., Poujois, A., Fabre, M., Lacaille, F., Debray, D., Rio, M., Fenaille, F., Cholet, S., Ruel, C., Caussé, E., et al. (2018). CCDC115-CDG: A new rare and misleading inherited cause of liver disease. Mol. Genet. Metab. *124*, 228–235.

27. Balasubramanian, M., Hurst, J., Brown, S., Bishop, N.J., Arundel, P., DeVile, C., Pollitt, R.C., Crooks, L., Longman, D., Caceres, J.F., et al.; DDD Study (2017). Compound heterozygous variants in NBAS as a cause of atypical osteogenesis imperfecta. Bone *94*, 65–74.

28. Segarra, N.G., Ballhausen, D., Crawford, H., Perreau, M., Campos-Xavier, B., van Spaendonck-Zwarts, K., Vermeer, C., Russo, M., Zambelli, P.Y., Stevenson, B., et al. (2015). NBAS mutations cause a multisystem disorder involving bone, connective tissue, liver, immune system, and retina. Am. J. Med. Genet. A. *167A*, 2902–2912.

29. Maksimova, N., Hara, K., Nikolaeva, I., Chun-Feng, T., Usui, T., Takagi, M., Nishihira, Y., Miyashita, A., Fujiwara, H., Oyama, T., et al. (2010). Neuroblastoma amplified sequence gene is associated with a novel short stature syndrome characterised by optic nerve atrophy and Pelger-Huët anomaly. J. Med. Genet. *47*, 538–548.

30. Palagano, E., Zuccarini, G., Prontera, P., Borgatti, R., Stangoni, G., Elisei, S., Mantero, S., Menale, C., Forlino, A., Uva, P., et al. (2018). Mutations in the Neuroblastoma Amplified Sequence gene in a family affected by Acrofrontofacionasal Dysostosis type 1. Bone *114*, 125–136.

31. Arasaki, K., Takagi, D., Furuno, A., Sohda, M., Misumi, Y., Wakana, Y., Inoue, H., and Tagaya, M. (2013). A new role for RINT-1 in SNARE complex assembly at the trans-Golgi network in coordination with the COG complex. Mol. Biol. Cell *24*, 2907–2917.

32. Aoki, T., Ichimura, S., Itoh, A., Kuramoto, M., Shinkawa, T., Isobe, T., and Tagaya, M. (2009). Identification of the neuroblastoma-amplified gene product as a component of the syntaxin 18 complex implicated in Golgi-to-endoplasmic reticulum retrograde transport. Mol. Biol. Cell *20*, 2639–2649.

33. Hirose, H., Arasaki, K., Dohmae, N., Takio, K., Hatsuzawa, K., Nagahama, M., Tani, K., Yamamoto, A., Tohyama, M., and Tagaya, M. (2004). Implication of ZW10 in membrane trafficking between the endoplasmic reticulum and Golgi. EMBO J. *23*, 1267–1278.

34. Schmitt, H.D. (2010). Dsl1p/Zw10: common mechanisms behind tethering vesicles and microtubules. Trends Cell Biol. *20*, 257–268.

35. Arasaki, K., Taniguchi, M., Tani, K., and Tagaya, M. (2006). RINT-1 regulates the localization and entry of ZW10 to the syntaxin 18 complex. Mol. Biol. Cell *17*, 2780–2788.

36. Nakajima, K., Hirose, H., Taniguchi, M., Kurashina, H., Arasaki, K., Nagahama, M., Tani, K., Yamamoto, A., and Tagaya, M. (2004). Involvement of BNIP1 in apoptosis and endoplasmic reticulum membrane fusion. EMBO J. *23*, 3216–3226.

37. Sun, Y., Shestakova, A., Hunt, L., Sehgal, S., Lupashin, V., and Storrie, B. (2007). Rab6 regulates both ZW10/RINT-1 and conserved oligomeric Golgi complex-dependent Golgi trafficking and homeostasis. Mol. Biol. Cell *18*, 4129–4142.

38. Raote, I., Ortega-Bellido, M., Santos, A.J., Foresti, O., Zhang, C., Garcia-Parajo, M.F., Campelo, F., and Malhotra, V. (2018). TANGO1 builds a machine for collagen export by recruiting and spatially organizing COPII, tethers and membranes. eLife *7*, 7.

39. He, S., Ni, D., Ma, B., Lee, J.H., Zhang, T., Ghozalli, I., Pirooz, S.D., Zhao, Z., Bharatham, N., Li, B., et al. (2013). PtdIns(3)P-bound UVRAG coordinates Golgi-ER retrograde and Atg9 transport by differential interactions with the ER tether and the beclin 1 complex. Nat. Cell Biol. *15*, 1206–1219.

40. Mizushima, N., and Komatsu, M. (2011). Autophagy: renovation of cells and tissues. Cell *147*, 728–741.

41. van der Vaart, A., Griffith, J., and Reggiori, F. (2010). Exit from the Golgi is required for the expansion of the autophagosomal phagophore in yeast Saccharomyces cerevisiae. Mol. Biol. Cell *21*, 2270–2284.

42. Cinque, L., Forrester, A., Bartolomeo, R., Svelto, M., Venditti, R., Montefusco, S., Polishchuk, E., Nusco, E., Rossi, A., Medina, D.L., et al. (2015). FGF signalling regulates bone growth through autophagy. Nature *528*, 272–275.

43. González-Rodríguez, A., Mayoral, R., Agra, N., Valdecantos, M.P., Pardo, V., Miquilena-Colina, M.E., Vargas-Castrillón, J., Lo Iacono, O., Corazzari, M., Fimia, G.M., et al. (2014). Impaired autophagic flux is associated with increased endoplasmic reticulum stress during the development of NAFLD. Cell Death Dis. *5*, e1179.

44. Tanaka, S., Hikita, H., Tatsumi, T., Sakamori, R., Nozaki, Y., Sakane, S., Shiode, Y., Nakabori, T., Saito, Y., Hiramatsu, N.,

et al. (2016). Rubicon inhibits autophagy and accelerates hepatocyte apoptosis and lipid accumulation in nonalcoholic fatty liver disease in mice. Hepatology *64*, 1994–2014.

45. Willy, J.A., Young, S.K., Mosley, A.L., Gawrieh, S., Stevens, J.L., Masuoka, H.C., and Wek, R.C. (2017). Function of inhibitor of Bruton's tyrosine kinase isoform α (IBTKα) in nonalcoholic steatohepatitis links autophagy and the unfolded protein response. J. Biol. Chem. *292*, 14050–14065.

46. Bartolomeo, R., Cinque, L., De Leonibus, C., Forrester, A., Salzano, A.C., Monfregola, J., De Gennaro, E., Nusco, E., Azario,
I., Lanzara, C., et al. (2017). mTORC1 hyperactivation arrests bone growth in lysosomal storage disorders by suppressing autophagy. J. Clin. Invest. *127*, 3717–3729.

47. Otterpohl, K.L., and Gould, K.A. (2017). Evaluation of Rint1 as a modifier of intestinal tumorigenesis and cancer risk. PLoS ONE *12*, e0172247.

48. Li, N., Thompson, E.R., Rowley, S.M., McInerny, S., Devereux, L., Goode, D., Investigators, L., Wong-Brown, M.W., Scott, R.J., Trainer, A.H., et al. (2016). Reevaluation of RINT as a breast cancer predisposition gene. Breast Cancer Res. Treat. *159*, 385–392.